



## MINING MACHINERY, TRANSPORT, AND MECHANICAL ENGINEERING


Research paper

<https://doi.org/10.17073/2500-0632-2022-12-67>

УДК 621.23.05

**Justification of the air distribution system of a down-the-hole hammer with an efficient operating cycle**P. N. Tambovtsev   , E. P. Rusin  

N.A. Chinakal Institute of Mining of the Siberian Branch of the RAS, Novosibirsk, Russian Federation

 [tambovskiyp@mail.ru](mailto:tambovskiyp@mail.ru)**Abstract**

One method for conserving energy in the mining industry and ensuring the required pressure of compressed air in underground mining networks is to decrease the specific energy carrier consumption, particularly in the case of down-the-hole hammers. The objective of this study is to substantiate the air distribution system of an air hammer, aimed at reducing the specific consumption of compressed air. We propose a system consisting of two chambers with a constant supply of compressed air, two controllable chambers, two elastic valves on the hammer, and a valve for cutting off the supply of compressed air to the forward stroke chamber, which is controlled by the hammer's position. This proposed configuration was employed to create two different designs for the air hammer. The operational cycle of the designed device has been numerically examined using SimulationX software and validated through experimental testing on a laboratory bench. Our calculations reveal that the suggested air distribution system, featuring controlled inlet to the backward stroke chamber, successfully achieves the stated objective. In comparison to the standard M29T hammer with nearly identical dimensions, striking power, and compressed air consumption for cleaning the borehole, the designed hammer exhibits a 53% reduction in specific energy consumption, and its electrical power usage for compressed air supply is halved. These design specifications align with both experimental results and data derived from the existing literature, confirming the accuracy of our calculation.

**Keywords**

energy consumption, down-the-hole hammer, air distribution system, specific consumption, percussion power, bottomhole purging, numerical simulation, operating cycle parameters, bench experiments

**For citation**


Tambovtsev P.N., Rusin E.P. Justification of the air distribution system of a down-the-hole hammer with an efficient operating cycle. *Mining Science and Technology (Russia)*. 2023;8(4):360–376. <https://doi.org/10.17073/2500-0632-2022-12-67>

## ГОРНЫЕ МАШИНЫ, ТРАНСПОРТ И МАШИНОСТРОЕНИЕ

Научная статья

**Обоснование системы воздухораспределения погружного пневмоударника с экономичным рабочим циклом**П. Н. Тамбовцев   , Е. П. Русин  

Институт горного дела им. Н.А. Чинакала СО РАН (ИГД СО РАН), г. Новосибирск, Российская Федерация

 [tambovskiyp@mail.ru](mailto:tambovskiyp@mail.ru)**Аннотация**

Одним из способов экономии энергии в горной промышленности и обеспечения необходимой величины давления сжатого воздуха в воздухопроводных сетях подземных добычных предприятий является уменьшение удельного расхода энергоносителя потребителями, в частности, погружными пневмоударниками. Цель настоящей работы – обоснование системы воздухораспределения пневмоударника, обеспечивающей снижение удельного расхода сжатого воздуха. Предложена система, включающая две камеры с постоянной подачей сжатого воздуха, две управляемые камеры, два упругих клапана на ударнике и клапан для отсечки подачи сжатого воздуха в камеру прямого хода, управляемые от положения ударника. На основе предложенной конфигурации разработаны два варианта конструкции пневмоударника. Рабочий цикл разработанного устройства исследован численно с привлечением программно-



го обеспечения SimulationX и экспериментально на лабораторном стенде. Расчеты показали, что предложенная система воздухораспределения в версии с управляемым впуском в камеру обратного хода обеспечивает достижение поставленной цели. По сравнению с серийным пневмоударником M29T, при практически одинаковых с ним габаритах, ударной мощности, расходе сжатого воздуха на продувку забоя скважины, разработанный пневмоударник имеет удельный расход энергоносителя на 53 % меньше, а потребление электрической мощности на его питание сжатым воздухом в 2 раза ниже. Расчетные данные соответствуют опытным, полученным в эксперименте и из литературных источников, что подтверждает корректность результатов расчета.

#### Ключевые слова

энергопотребление, погружной пневмоударник, система воздухораспределения, удельный расход, ударная мощность, продувка забоя скважины, численное моделирование, показатели рабочего цикла, стендовые эксперименты

#### Для цитирования

Tambovtsev P.N., Rusin E.P. Justification of the air distribution system of a down-the-hole hammer with an efficient operating cycle. *Mining Science and Technology (Russia)*. 2023;8(4):360–376. <https://doi.org/10.17073/2500-0632-2022-12-67>

### Introduction

The mining industry stands as one of the primary consumers of energy resources. Therefore, the conservation of energy during various operational processes within the industry holds significant importance. Moreover, energy management efforts should be directed towards diminishing energy intensity [1]. This notion is particularly relevant to one of the fundamental processes in mining, which is drilling. Thus, there arises a need to enhance the energy efficiency of air percussion drilling in domestic mines [2–4].

It is imperative to note that the majority of underground mines and shafts operating in Russia currently fail to maintain the required level of compressed air pressure within their air networks. One of the contributing factors to this issue is the excessive energy consumption of pneumatic mining equipment, surpassing the technical capabilities of compressor stations. Consequently, the air network's pressure drops below 0.5 MPa, negatively impacting the efficiency of operational processes [5], including drilling activities.

One effective approach to address these challenges involves the reduction of specific compressed air consumption in down-the-hole hammers (DTH hammers). In the context of DTH hammers, specific consumption pertains to the volume of compressed air needed to generate one unit of percussion energy. Table 1 compiles the principal technical data concerning domestic DTH hammers. Most widely known, mass-produced machines feature either a valve or spoolless type of air distribution, resulting in specific consumption rates of  $(37.0–49.4) \times 10^{-6} \text{ m}^3/\text{J}$ . Some spoolless-type air hammers, like the PV-170, allow for a slight reduction in specific consumption while maintaining high percussion energy. Nevertheless, this reduction comes at the cost of a significant decrease in percussion frequency and overall percus-

sion<sup>1</sup> [6]. Notably, commercially available down-the-hole hammers with a spool-operated air distribution system are conspicuously absent. Prototypes featuring a combined air distribution system, such as the P105-1K, P105-2K<sup>2</sup>, P-110-3,5, and P110-EN<sup>3</sup>, were developed at the Institute of Mining of the Siberian Branch of the Russian Academy of Sciences. These prototypes have exhibited notable improvements in their technical characteristics [7, 8].

Internationally, DTH hammers are manufactured in several countries, including Sweden (Atlas Copco<sup>4</sup> [12], Sandvik<sup>5</sup>), USA (Rockmore International<sup>6</sup>), Great Britain (Halco Rock Tools<sup>7</sup>), China (Change ENYU Engineering Equipment Co. Ltd.<sup>8</sup>), India (SVE

<sup>1</sup> Alexeyev S.E. Down-the-hole pneumatic percussion mechanism. 2090730 (RF Patent), published in Bulletin of Inventions No. 26, 1997.

<sup>2</sup> Gaun V.A. Pneumatic percussion mechanism. Patent 998740 (USSR certificate of authorship). Published in Bulletin of Inventions No. 7, 1983.

<sup>3</sup> Lipin A.A., Belousov A.V., Zabolotskaya N.N. Down-the-hole hammer. 2252996 (RF Patent). Published in Bulletin of Inventions No. 15, 2005.

<sup>4</sup> Secoroc Rock Drilling Tools. Product catalogue – DTH equipment. Atlas Copco. URL: [https://atlas-co.ru/files/pdf/core\\_drilling/9851%206545%2001\\_L.pdf](https://atlas-co.ru/files/pdf/core_drilling/9851%206545%2001_L.pdf); Atlas Copco Secoroc. Technical specifications DTH Hammers. URL: <https://disk.yandex.ru/i/DgE7PG25o11AXA/>

<sup>5</sup> Sandvik RH560 3.5", 4", 5" and 6" DTH Hammers. URL: <https://www.rocktechnology.sandvik/en/products/rock-tools/down-the-hole-drilling-tools/down-the-hole-hammers/rh560-down-the-hole-hammers/>

<sup>6</sup> Down-the-hole hammers. RockMore International. URL: <https://www.rockmore-intl.com/download/61/dth-product-information-downloads/816/dth-hammers-catalog-section-4.pdf>

<sup>7</sup> Halco Rock Tools. Hammers (Unite Kingdom, Halco Brighthouse Ltd). URL: <https://www.halco.uk/hammers/>

<sup>8</sup> Changsha ENYU Engineering Equipments Co. Ltd (China). DTH hammer. URL: <http://www.enyudrill.com/pclass/?classa=1&classb=1>



Drilling Tools Pvt. Ltd.<sup>9</sup>), and others. majority of foreign prototypes feature spoolless air distribution, extended percussion components (piston, bit), and are pressure-operated (1.0–2.5 MPa). The key technical data for DTH hammers produced abroad is presented

<sup>9</sup> SVE Drilling Tools Pvt. Ltd. DH 01 Hammers (India). URL: <http://www.svedrillingtools.in/dh01-hammers.php>

in Table 2. Atlas Copco and Sandvik air hammers are industry leaders, outperforming their Russian counterparts in terms of percussion power. However, it's important to note that they operate at higher pressures (1.0–2.5 MPa), which may not be suitable for the conditions prevalent in most Russian mining enterprises.

Table 1

Specifications of domestic air hammers

Parameters	Domestic air hammers						
	M29T [9] / (P85-2)	M48 (P105PMK) <sup>1</sup> [9]	P155 (M32k) [10]	P105K [11]	P125 [11] / (P130-4m)	P105-1K [7]	P105-2k (M74u) <sup>2</sup> [7]
Air distribution type	Valve-operated			Spoolless		Combined	
Pressure $p$ , MPa	0,5 / 0,7	0.5	0.5	0.5	0.5 / 0.7	0.5	0.5
Percussion energy $A$ , J	54 / 91	93	178	96	150 / 182	194	206
Percussion frequency $f$ , Hz	25 / 22	28.3	23	26.7	20,8 / 22	16.3	16.1
Total air consumption $Q$ , m <sup>3</sup> /min	4.0 / 4.8	7.0	9.7	5.7	7.0 / 8.8	6.4	6.6
Percussion power $N$ , kW	1.35 / 2.0	2.63	4.1	2.56	3.12 / 4.0	3.17	3.32
Hammer mass $m$ , kg	1.75 / –	2.80	5.5	3.0	5.6 / –	4.45	4.45
Machine mass $M$ , kg	10 / 15	16.1	35.5	21.0	31.0 / 33.2	18.2	18.2
Specific power, W/kg	135 / 134	160	120	120	101 / 120	174	182
Dimensions (without bit): length, mm diameter, mm	549 / 622 70 / 80	(470) 92	459 140	615 92	(566) / 657 110 / 116	594 96	594 96
Bit diameter, mm	85 / 85	105	155	105	125 / 130	105	105
Specific air consumption $q$ , m <sup>3</sup> /J* ( $\times 10^{-6}$ )	49.4 / 40	45	39	37	37 / 37	34	33

\* The specific consumption of the air hammer is given with account of compressed air intake for borehole purging.

<sup>1</sup> Zinovyev A.A., Semenov L.I. Drill hammer. Patent 112867 (USSR certificate of authorship). 1958.

<sup>2</sup> Gaun V.A. Pneumatic percussion mechanism. Patent 998740 (USSR certificate of authorship). Published in Bulletin of Inventions No. 7, 1983.

Table 2

Specifications of foreign air hammers

Parameters	Model					
	USA		Sweden			
	(Rockmore International)		Sandvik		Atlas Copco (Secoroc)	
	ROK 2LT	ROK-3	RH560 3,5"	RH560 g4"	COP-34	COP-44
Air distribution type	–		–		Spoolless	
Pressure $p$ , MPa	0.6 / 1.04	0.6 / 2.4	1.0 / 1.8 / 2.4	1.0 / 1.8 / 2.4	1.05 / 2.5	1.05 / 2.5
Percussion energy $A$ , J	–	–	–	–	154 / 317	296 / 514
Percussion frequency $f$ , Hz	–	–	–	–	26 / 41	23.7 / 35
Air consumption $Q$ , m <sup>3</sup> /min	2.0 / 3.8	3.1 / 14.5	4,5 / 8.3 / 11.1	6.7 / 12.5 / 16.9	4.8 / 15.0	5.46 / 16.9
Power $N$ , kW	–	–	–	–	4.0 / 13.0	7.0 / 18.0
Hammer mass $m$ , kg	–	–	5.3	8.5	4.8	7.1
Hammer diameter $d$ , mm	–	–	–	–	–	78
Machine mass $M$ , kg (w/o bit)	(13)	(22)	(29)	(48)	27	38
Specific power, W/kg	–	–	–	–	148 / 481	184 / 474
Dimensions: length, mm (w/o bit) diameter, mm (w/o bit)	(840) (62)	(750) (82)	1004 (914) 85	1140 (1016) 105	1025 (83.5)	1034 (98)
Bit diameter, mm	70, 76	85, 105	85	105	105	110, 125
Specific air $q$ , m <sup>3</sup> /J ( $\times 10^{-6}$ )	–	–	–	–	20.0 / 19.2	13.0 / 15.6



### Research Aim, Objectives, and Methods

The aim of this study is to substantiate the air distribution system of an air hammer, with the goal of reducing the specific consumption of compressed air.

Research objectives:

- conducting a numerical investigation into the dynamics of working processes in typical air percussion systems, performing a comparative analysis of their efficiency for light-type DTH hammers, and identifying factors that hinder their efficiency;
- selecting an air distribution system and structural layout capable of mitigating the factors that negatively impact the consumption parameters of DTH hammers;
- developing the design of the air hammer, with the determination of its key dimensions;
- employing simulation modeling to explore the working process of a new DTH hammer and selecting the most suitable combination of design parameters to ensure the realization of the operating cycle with reduced specific consumption;
- estimating the compressed air consumption required for cleaning the bottomhole;
- experimentally verifying the reliability of the results obtained from numerical simulations of the air hammer;
- summarizing and evaluating the findings of the research.

Numerical (simulation) modeling of the working process within the air systems of DTH hammers was conducted using the SimulationX software<sup>10</sup>. The software's calculation module relies on a mathematical model [13, 14] that characterizes the dynamics of the percussion system. This model has demonstrated its adequacy and effectiveness in the analysis of a broad spectrum of air percussion devices [3]. The design diagram of the air percussion system encompasses generalized depictions of air connections and mechanical connections. The air connections diagram delineates the architecture of the air component, including the number of chambers, the interconnecting channels, and the presence of moving components that interact with these chambers. Channels connecting the chambers are specified by the flow cross-sectional area. Adjustable channels are characterized by diagrams illustrating changes in flow area. The mechanical connections diagram illustrates the nature of power interactions, which may involve elastic couplings, friction, and other relevant factors. Additionally, it accounts for percussion interactions between moving components, assuming them to be instantaneous

and describing them based on the concept of velocity recovery coefficients. The software utilizes the given initial conditions to calculate displacements and velocities of the moving components, along with pressure and temperature within the chambers, and the instantaneous mass flow rate of compressed air. The outcomes are presented in the form of operational cycle diagrams, showcasing factors such as chamber pressure, velocity and displacement of moving components, and the rate of compressed air flow within channels. Specific characteristics of the calculations are elucidated below.

A comparative analysis of the efficiency of air percussion systems for lightweight DTH hammers with similar dimensions and percussion power involves identifying the system with the lowest specific consumption of compressed air.

Physical experiments are carried out using a laboratory prototype of an air hammer. These experiments make use of measurement equipment, including a laboratory bench and an array of recording devices. Further details regarding this equipment and the methodology for conducting experimental work are expounded upon in the relevant section below.

### Numerical Study of the Working Process Dynamics in Typical Air Percussion Systems for Lightweight DTH Hammers

The objective of this study is to assess the efficiency of typical air percussion systems in terms of specific energy consumption and percussion power for DTH hammers with a body diameter of 70 mm, categorizing them as lightweight models.

The investigation considered three primary types of air distribution systems commonly used in the design of air percussion devices [9, 10]: valve-operated (M29T), spoolless (P125), and spool-operated (PN-1300). As a baseline for comparison, a commercially available valve-type lightweight DTH hammer, the M29T, was selected. The two other systems, spoolless and spool-operated, were configured as air hammers with geometric and mass-dimension parameters scaled down to match those of the baseline. Consequently, identical values for the key parameters were established for all three selected air percussion mechanisms:  $L$  (the length of the air hammer),  $D$  (the outer diameter of the body or cylinder),  $m_1$  (the mass of the hammer),  $S$  (the effective area of the hammer),  $H_o$  (the overall stroke of the hammer), and  $p_m$  (the operating pressure in the main line). Variations in other parameters, encompassing the volumes of working chambers, cross-sectional areas of air passages, and air distribution coordinates, were systematically adjusted to ensure the congruence of the

<sup>10</sup> ESI Group. System Simulation Software. SimulationX. URL: <https://www.esi-group.com/products/system-simulation>



operational cycle diagrams of the DTH hammer's typical air percussion mechanisms with those observed in actual machines. In the subsequent sections, the working chambers are referred to as follows: the forward stroke chamber – FSC and the backward stroke chamber – BSC.

The designs of the considered models of down-the-hole air hammers with typical air percussion systems are presented in Fig. 1, and their operating principle and working process features are described in [11, 13, 17]. Construction diagrams (Fig. 1, *a, b, c*) illustrate the moving components of these systems, set at the origin of coordinates (hammer at the

moment of percussion). In this configuration, the initial chamber volumes, air distribution window coordinates, and the range of movement for these components are all ascertained.

In Fig. 2 the generalized design diagrams of typical air percussion systems are demonstrated. Each chamber and its associated moving mass are designated with a serial number, such as chamber  $V_i$ , mass  $m_i$ . The clear area between chamber 1 and chamber 2 is conventionally labeled by  $J_{12}$ , while the effective area of the moving components, like hammer  $m_1$  on the side of chamber  $V_2$ , is represented by  $S_{21}$ . The modifications in flow cross-sections

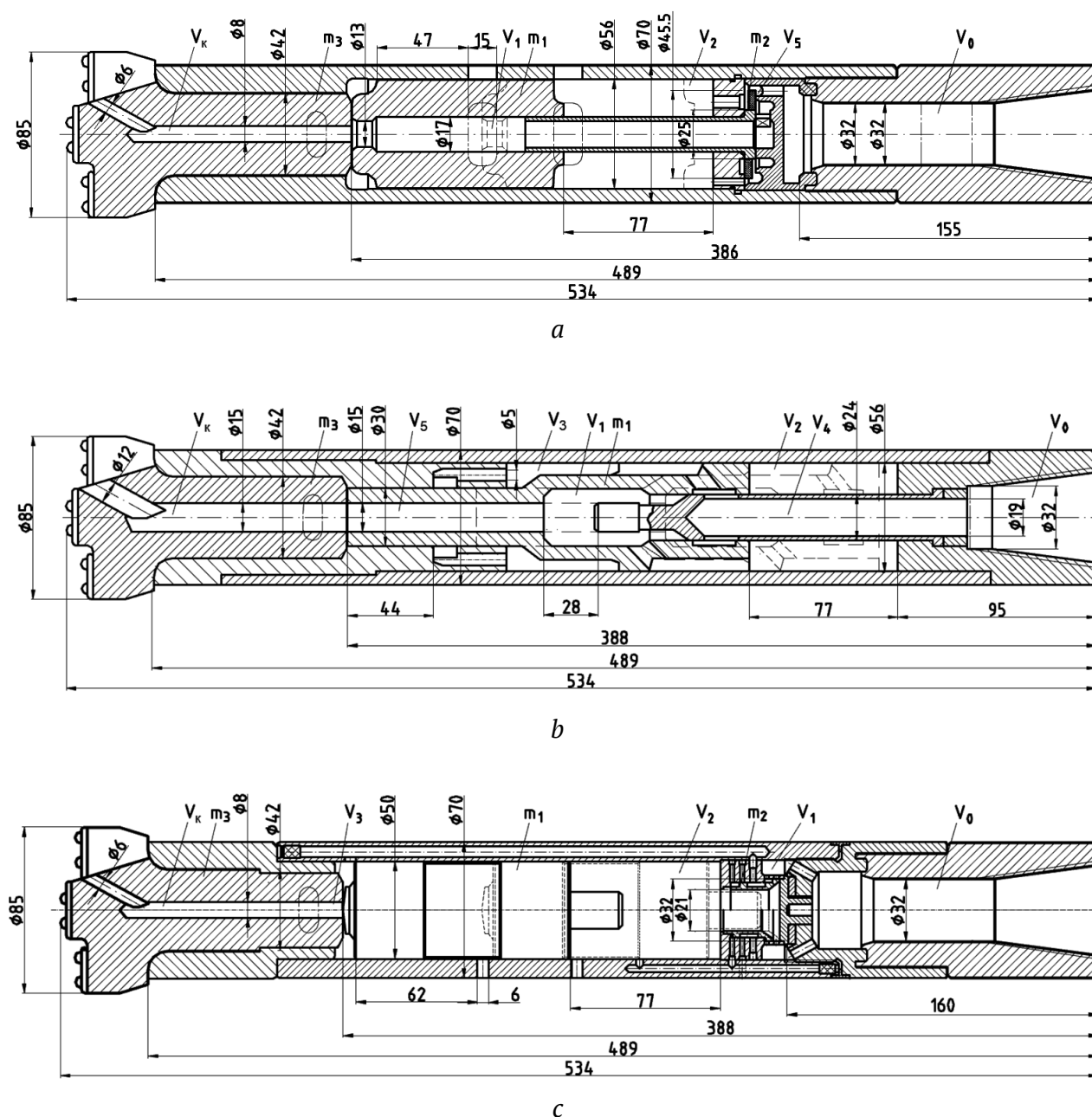


**Fig. 1.** Layout and main structural dimensions of air hammers with typical air distribution systems: *a* – valve-operated (M29T [9]), *b* – spoolless (P125 [11]), *c* – spool-operated (PN-1300 [11, 15])

that correspond to the positions of hammer 1 and the distributing components (valve or spool) are described in a similar fashion [14]. The pneumatic resistances within the channels are accounted for using flow coefficients ( $k_f = 0.4 \dots 0.6$ ). The essential design parameters, initial pressures in the chambers, and velocity recovery coefficients have been incorporated into the design model. The evaluation of the working process is based on the structure of the operating cycle diagrams and the values of output indicators, encompassing parameters such as the energy and frequency of percussions, compressed air consumption, and their respective derived values, as well as the working stroke of the hammer. The pursuit of optimal configurations for air distribution systems was carried out with the objective of minimizing specific compressed air consumption. This involved

adjusting the working volumes of chambers, the areas of air passage cross-sections, the coordinates where moving components interact, and the masses of valves, guided by this criterion.

Design diagrams of typical air percussion systems are presented in Fig. 3, depicting pressure, displacement, and velocity of moving components, the instantaneous mass flow rate. These diagrams correspond to the design parameter values and initial calculation conditions outlined in Table 3. The calculations reveal that the hammer is provided the percussion velocity within permissible limits, reaching up to 8.43 m/s, along with the necessary operating stroke of the hammer (65–68 mm) and a suitably high frequency of percussions (22.2–27.8 Hz). Table 3 presents the design output indicators for typical air percussion systems.

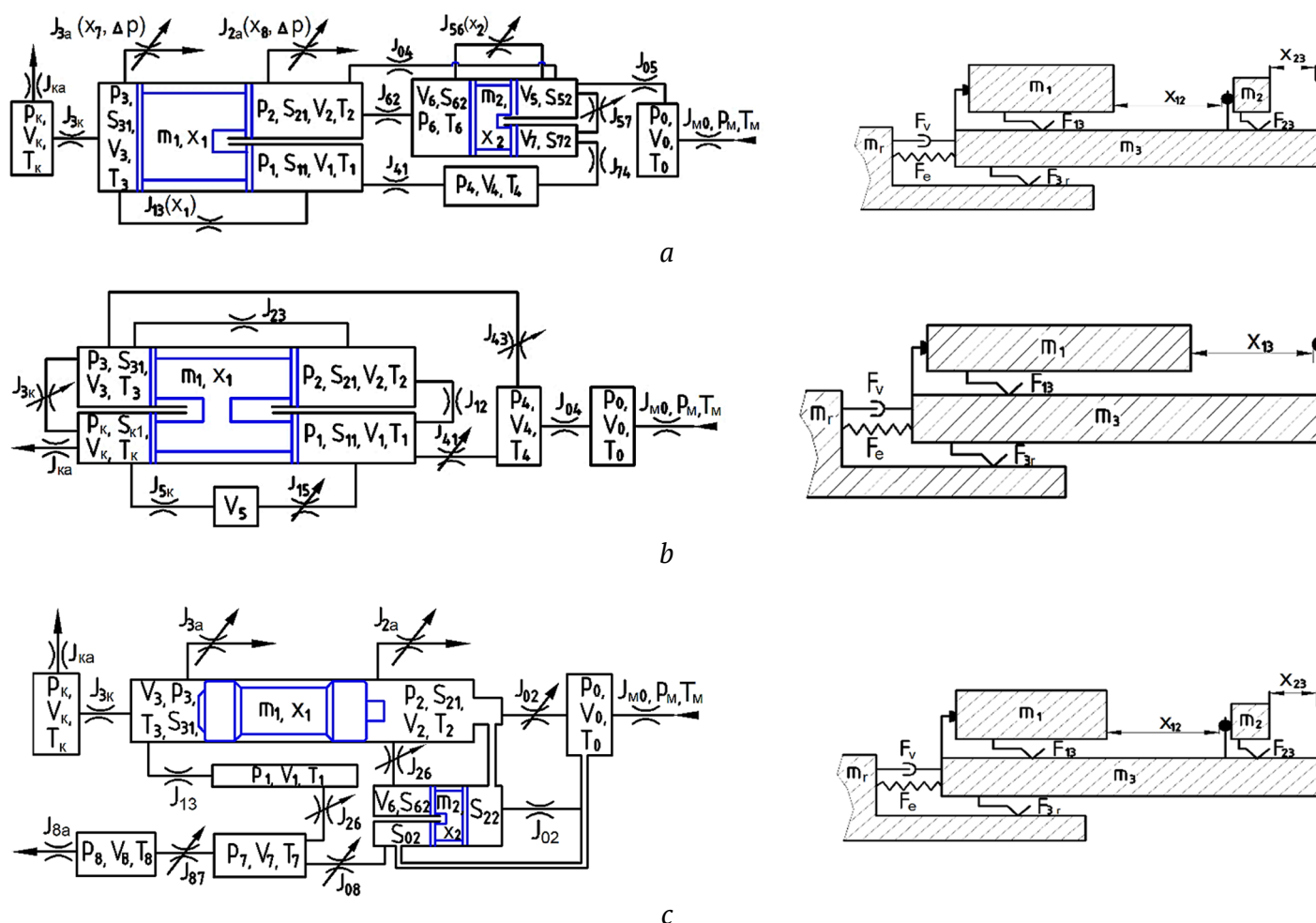


**Fig. 2.** Generalized design diagrams (pneumatic, mechanical) of typical air percussion systems: *a* – valve-operated (prototype M29T); *b* – spoolless (P125); *c* – spool-operated (PN-1300):  $V_i$  – volumes of chambers;  $J_{m0}$  – area of the air passage cross-section of the main line;  $J_{ij}$ ,  $J_{ia}$  – areas of air passage cross-sections between the  $i$ -th and  $j$ -th chambers, between the  $i$ -th chamber and atmosphere;  $m_i$ ,  $x_i$  – masses and coordinates of moving components (hammer, valves,  $m_r$  – rock);  $S_{ij}$  – effective areas of components  $m_i$  from the side of the  $j$ -th chamber;  $T_i$ ,  $T_m$  – absolute temperature of compressed air in the  $i$ -th chamber and in the main line;  $p_m$ ,  $p_i$ ,  $p_a$  – absolute pressure of compressed air in the main line,  $i$ -th chamber and in the atmosphere;  $F_e$ ,  $F_v$  – forces of elastic-damping connection of the air hammer with the rock;  $F_{13}$ ,  $F_{5r}$ ,  $F_{23}$  – friction forces: hammer – body, body – rock, valve – body

The simulation demonstrates that all models of air hammers with typical air distribution systems operate stably at two main pressure values of 0.5/0.6 MPa. With similar mass-dimensional characteristics, the valve system (M29T) yields percussion power of 1.42/1.63 kW, while the valveless system provides 0.96/1.19 kW, and the spool system delivers 1.13/1.48 kW. Notably, the maximum percussion energy is achieved by the valve (54.0/60.0 J) and spool (51.2/60.2 J) systems, whereas the valveless system exhibits the lowest percussion energy at 36.4/42.8 J. In terms of specific consumption, the operating cycles of air hammers with spool and valveless types of air distribution systems ( $29.3/32.0 \times 10^{-6} \text{ m}^3/\text{J}$ ) are the most efficient. The specific consumption of the batch-produced air hammer M29T is 1.4/1.7 times higher than that of the other two typical systems.

Let us analyze the operating cycles of typical air percussion mechanisms using diagrams (see Fig. 3) and calculated output indicators (Table 3).

Regarding the valve-operated air hammer M29T, the actuation of the cross-over valve at specific intervals connects the main line to the atmosphere through channels, leading direct air leakage. In the FSC, just before the beginning of exhaust, there is elevated pressure (0.37 MPa). Prior to percussion, a pressure pulse occurs in the BSC, which reduces the percussion energy. These factors contribute to high specific compressed air consumption ( $q = 44.7 / 50.6 \times 10^{-6} \text{ m}^3/\text{J}$ ).

The spoolless air hammer, as depicted in the P125 diagram, introduces air into the working chambers through controllable channels, that are manipulated by the hammer's actions. It is evident from the diagrams (see Fig. 3, b) that the percussion power of the device decreases, and air consumption increases due to several factors: relatively high pressure in the FSC just before exhaust (0.43 MPa), a substantial initial volume of the BSC, and a notable pressure pulse in the BSC, which diminishes the kinetic energy of the hammer during the forward stroke. This air

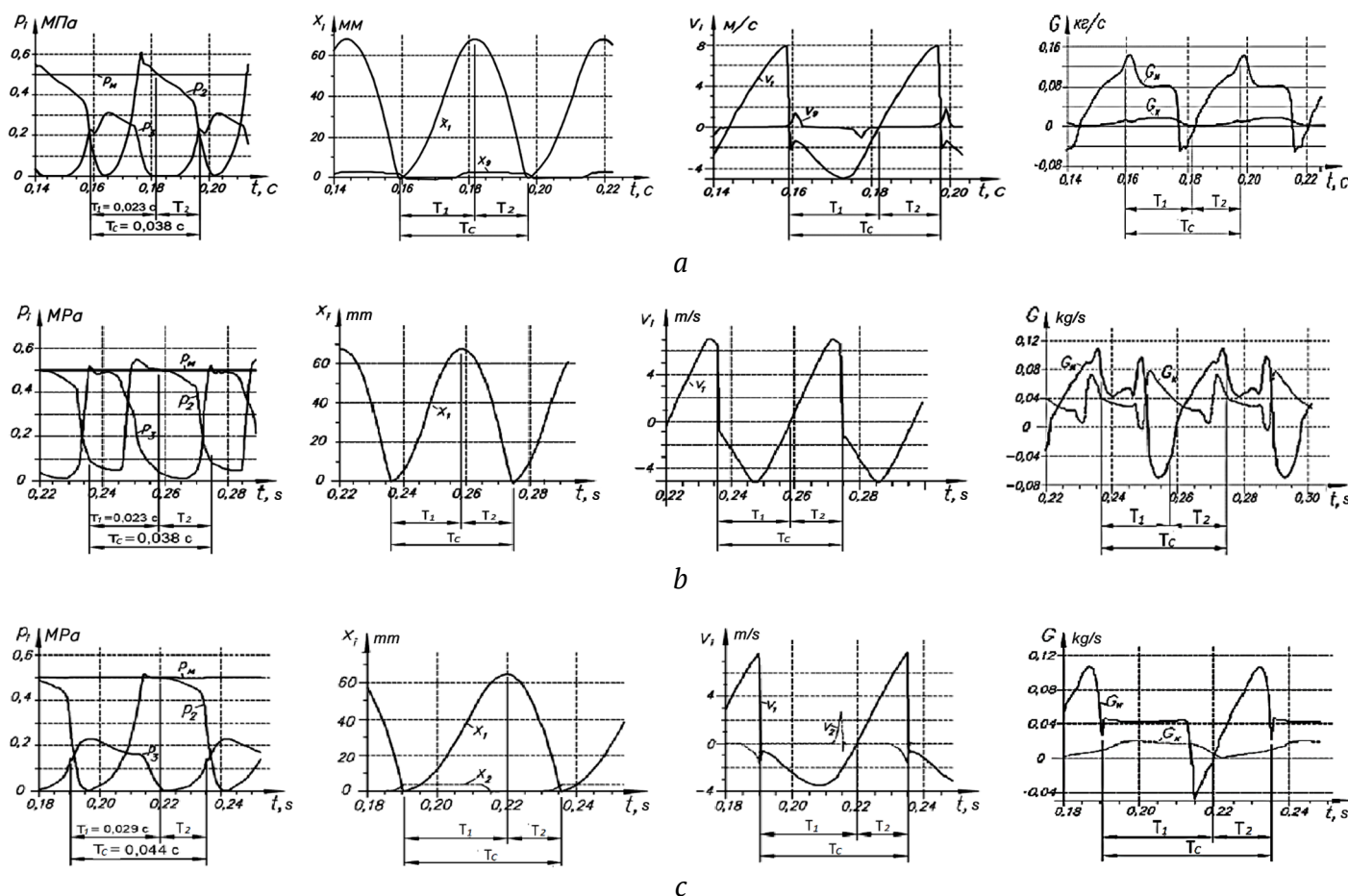


**Fig. 4.** Design diagrams of operating cycles (changes in compressed air pressure in time  $p_i(t)$  in the  $i$ -th chambers; displacement of hammer  $x_1$ , valve and spool  $x_2$ ; velocity of hammer  $v_1$ , valve and spool  $v_2$ , the instantaneous mass flow rate of compressed air  $G$ ) of the air hammer models with typical air distribution systems: *a* – valve-operated (M29T), *b* – spoolless (P125), *c* – spool-operated (PN-1300):  $v_1, v_2$  – velocity of the hammer, valve / spool respectively, m/s;  $x_1, x_2$  – displacement of the hammer, valve / spool respectively, m/s;  $G_m$  – flow rate through the main channel  $j_{m0}$ ;  $G_c$  – flow rate through the channel  $j_{cha}$  in the bit  $t$  – time, s;  $T_c$  – cycle period;  $T_1, T_2$  – periods of backward and forward strokes



hammer delivers a percussion power of 0.96 / 1.19 kW, a percussion energy of 36.4 / 42.8 J, and a specific consumption of 32.0 /  $31.1 \times 10^{-6} \text{ m}^3/\text{J}$ .

The *spool-operated air hammer according to the basic flow diagram of the PN-1300 air percussion machine* provides compressed air to the working chambers through channels in the body, with opening and closing managed by a spool. The spool's movement depends on the pressure within the working chambers and the pre-spool chamber. Notably, the BSC of this device holds the smallest volume (0.0134 dm<sup>3</sup>) as compared to 0.0950 dm<sup>3</sup> in the spoolless system and 0.0162 dm<sup>3</sup> in the valve-operated one. The maximum pressure in the BSC (0.23 MPa) also stands as the lowest (as opposed to 0.5 MPa in the spoolless system and 0.31 MPa in the valve-operated one), and the pressure just before exhaust registers at 0.16 MPa (versus 0.43 MPa in the spoolless system and 0.24 MPa in the

valve-operated one). These characteristics contribute to a reduction in compressed air consumption by the spool-operated air hammer.

During the direct stroke of the hammer, there is notably high average pressure (0.52–0.53 MPa) in the period preceding the beginning of exhaust from the FSC, while the pressure pulse in the BSC is reduced (with the pressure in the BSC at the moment of percussion not exceeded 1.4 MPa). Although the effective area of the hammer is smaller, this configuration results in higher percussion energy. However, concurrently, the high pressure in the FSC just before exhaust (0.43 MPa) and the large volume of the FSC lead to losses in the internal energy of compressed air. Among the three considered pneumatic percussion mechanisms, this specific consumption is the lowest ( $q = 31.7 / 29.3 \times 10^{-6} \text{ m}^3/\text{J}$ ), suggesting a significant margin for its further reduction.

Table 3

Design parameters of typical air percussion systems for light-weight DTH hammers

Prototype machine	M29T					
Air percussion system diagram	M29T		P125		PN-1300	
Air distribution type	Valve-operated		Spoolless		Spool-operated	
Specified parameters						
Overpressure $p$ , MPa	0.5	0.6	0.5	0.6	0.5	0.6
Bit diameter, mm	85		85		85	
Outer diameter of the body (cylinder), mm	70		70		70	
Total length of air hammer with bit $L$ , mm	534		534		534	
Internal diameter of cylinder, mm	56		56		50	
Hammer mass $m$ , kg	1.75		1.75		1.75	
Valve mass $m_2$ (spool $m^2$ ), kg	0.035		–		(0.036)	
Effective area of hammer (BSC/FSC) $S_{ij}$ , cm <sup>2</sup>	22.3 / 22.3		17.5 / 22.8		19.6 / 19.6	
Ratio of hammer effective area to cross-section area of body with a diameter of 70 mm	0.58		0.59		0.51	
Overall stroke $H_d$ , mm	77		77		77	
Flow rate coefficient $k_f$	0.5–0.6		0.5–0.6		0.5–0.6	
Velocity recovery coefficient $k_r$	0.10–0.15		0.10–0.15		0.10–0.15	
Stroke before exhaust from BSC, mm	47		38		62	
Chamber initial volumes: $V_1$ , dm <sup>3</sup> ; $V_2$ , dm <sup>3</sup> ; $V_3$ , dm <sup>3</sup> ; $V_4$ , dm <sup>3</sup>	0.0204; 0.1810; 0.0162; 0.0196		0.0280; 0.1600; 0.0950; 0.0410		0.0270; 0.1570; 0.0134; 0.0267	
Main line channel area $J_{m0}$ , cm <sup>2</sup>	8.04		8.04		8.04	
Hammer/cylinder clearance area, cm <sup>2</sup>	0.04		0.04		0.04	
Area of channel in bit $J_{cha}$ , cm <sup>2</sup>	0.502		2.010		0.502	
Output indicators						
Stroke velocity $v$ , m/s	7.86	8.28	6.45	7.00	7.65	8.43
Operating stroke $H_o$ , mm	67	68	67	68	65	66
Percussion energy $A$ , J	54.0	60.0	36.4	42.8	51.2	62.2
Percussion frequency $f$ , Hz	26.3	27.1	26.3	27.8	22.2	23.8
Cycle period $T_c$ , s	0.038	0.037	0.038	0.036	0.044	0.042
Percussion power $N$ , kW	1.42	1.626	0.96	1.19	1.13	1.48
Total air consumption $Q$ , m <sup>3</sup> /min	3.81	4.94	1.84	2.22	2.16	2.60
Air flow rate through bit channel $Q_b$ , m <sup>3</sup> /min	0.69	0.78	1.84	2.22	0.62	0.69
Specific air consumption $q$ , m <sup>3</sup> /J ( $\times 10^{-6}$ )	44.7	50.6	32.0	31.1	31.7	29.3





### Selection of air distribution systems and design diagrams of DTH hammers

Table 4 summarizes the main advantages and disadvantages of typical air percussion mechanisms, along with the factors that contribute to increased specific consumption and the methods identified through numerical simulation to reduce it.

Analysis of the operating cycles of typical air percussion systems has led to the establishment, that an effective air percussion system should fulfill:

1. Avoid continuous compressed air supply to working chambers; instead, control the compressed air inlet and exhaust.

2. Ensure that the effective area of the hammer on the FSC side is not less than 0.6 times the cross-sectional area of the air hammer.

3. Minimize resistance to the hammer's movement caused by air pressure from the respective working chambers.

4. Cut-off of compressed air supply to the working chambers before exhaust and provision of increased rate of compressed air expansion.

5. Keep the initial volume of the BSC relatively small.

6. Maintain a design simplicity.

From the above conditions, it becomes evident that reducing the specific compressed air consumption by an air hammer is achievable by eliminating resistance during both the forward and backward strokes of the hammer caused by air compression in the controllable working chambers

and by ensuring a greater degree of air expansion. One of the most effective and structurally simple components for meeting these requirements is the elastic valve<sup>11</sup> [7, 16], which was initially proposed by V.A. Gaun at the Institute of Mining of the Siberian Branch of the USSR Academy of Sciences. The use of elastic valves has led in a doubling of percussion energy and a 30% increase in percussion power for air hammers with the same diameter and compressed air consumption. Elastic valves offer several advantages due to their ease of integration into the machine design and their ability to provide a large air passage cross-section. These valves consist of a ring made of elastic material, such as rubber or plastic, placed in a groove on the hammer or the body of the air percussion mechanism. The ring can open or close the gap along the outer or inner diameter, depending on the pressure in the chambers communicating through this gap, ensuring the sealing of the working chamber or its connection with the atmosphere.

For the timely inlet and cut-off of compressed air supply to the FSC, an annular step inelastic valve, controlled by the hammer, can be employed. This valve allows for almost instantaneous full opening of the inlet cross-section to the chamber, just before the hammer changes direction. The efficiency of this solution has been confirmed through experimental studies [17].

<sup>11</sup> Gaun V.A. Pneumatic percussion mechanism. Patent 998740 (USSR certificate of authorship). Published in Bulletin of Inventions No 7, 1983.

Table 4

Comparative analysis of typical air percussion mechanisms

Air distribution system	Specific consumption ( $\times 10^{-6}$ ) m <sup>3</sup> /J	Advantages	Disadvantages	Main factors improving specific consumption	Ways to reduce the specific consumption and improve the design
Valve-operated (M29T)	44.7	High specific percussion power (W/kg), high frequency of percussions, design simplicity	High specific consumption	Inevitable direct overflow of compressed air from the main line to the atmosphere to activate the cross-over valve	Cut-off of compressed air supply to working chambers before exhaust; increase of the compressed air expansion rate in the chambers.
Spoolless (P125)	32.0	High percussion frequency, simple design	High specific consumption, low percussion energy; design complexity, low hammer durability and strength	Large initial volume of BSC, losses of internal energy with exhaust, resistance to hammer movement from air compression in the BSC, resistance in the FSC.	Elimination of constant supply of compressed air to the FSC; increase in the degree of expansion of compressed air in the BSC; elimination of stress concentrators in the hammer.
Spool-operated (PN-1300)	31.7	High percussion energy, integral hammer, reliable operation; no uncontrollable working chambers, reduced resistance to hammer stroke.	High specific consumption; complexity of manufacturing of the body (cylinder with channels).	Resistance to hammer movement from air compression in the FSC and BSC, low rate of expansion of compressed air in working chambers and losses of internal energy during exhaust; small working area of the hammer.	Elimination of internal energy losses of compressed air with exhaust; simplification of body design, elimination of resistance to hammer stroke from air compression in the BSC at the end of the hammer forward stroke

Controlling the supply of compressed air to the BSC can be more easily achieved by using a channel in the hammer controlled by its position. An alternative, simpler approach is to maintain a constant air inlet to the BSC through a throttle hole in the hammer.

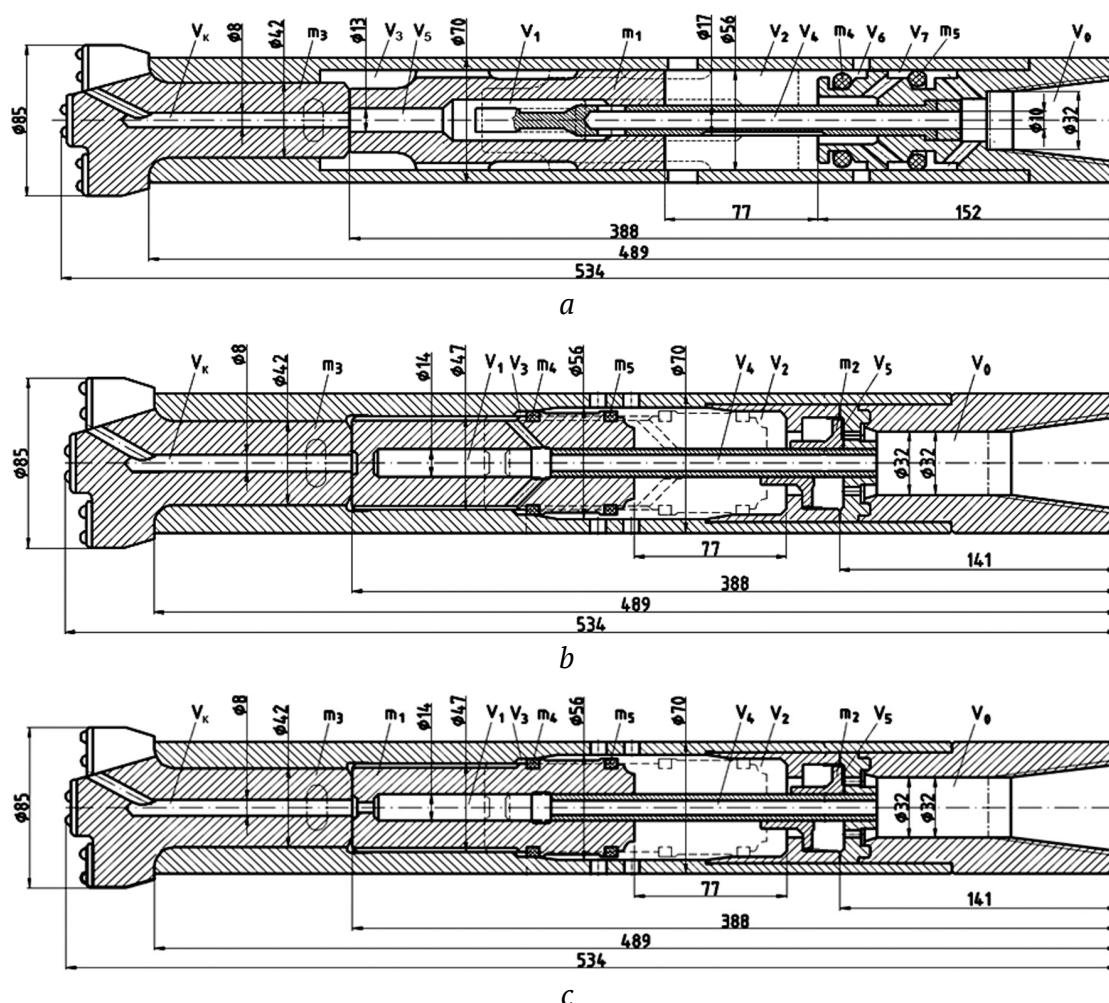
Typical air percussion systems do not fully realize the proposed methods for reducing specific consumption (see Table 4). Therefore, we use combined air hammer diagrams that incorporate elastic ring valves (Fig. 4). The starting point is the diagram of the two-valve air hammer P105-2K<sup>12</sup> [7] (Fig. 4, *a*), which has twice the percussion energy compared to analogs with the same compressed air consumption. This diagram's distinct feature is that during the backward stroke, elastic valves  $m_4$  and  $m_5$  connect the BSC with the atmosphere, effectively eliminating resistance to the hammer's movement<sup>13</sup>.

<sup>12</sup> Gaun V.A. Pneumatic percussion mechanism. Patent 998740 (USSR certificate of authorship). Published in Bulletin of Inventions No 7, 1983.

<sup>13</sup> I bid.

Figs. 4, *b*, and *c* provide new diagrams that allow for the implementation of the proposed methods to reduce specific consumption (see Table 4). In these diagrams, in contrast to the P105-2K diagram (Fig. 4, *a*), the use of two elastic valves ( $m_4$ ,  $m_5$ ) on the hammer ( $m_1$ ) eliminates pneumatic resistance during not only the backward but also the forward stroke.

The air hammer shown in Fig. 4, *b* employs air distribution system K1 (valve-spoolless) with a controllable channel in the hammer. In Fig. 4, *c*, it utilizes system K2 (valve-throttle-operated) with a throttle channel in the hammer. The air inlet to chamber  $V_2$  from main line  $V_0$  occurs at the end of the backward stroke of hammer  $m_1$  when valve  $m_2$  is actuated, overriding its displacement by the hammer. Exhaust from chamber  $V_2$  takes place at the end of the forward stroke through exhaust windows in the cylinder. Compressed air is introduced into the chamber  $V_3$  through channel  $V_4$  in the nozzle, chamber  $V_1$ , the channel





in the hammer, and exhaust is conducted through side windows in the cylinder and channel  $V_b$  in the bit. Valve  $m_4$  seals working chamber  $V_3$  during the backward stroke of the hammer, and valve  $m_5$  seals chamber  $V_2$  during the forward stroke. Valve  $m_2$  increases the reliability of the air percussion mechanism by ensuring stable air inlet into the controllable forward stroke chamber  $V_2$  at the end of the hammer's backward stroke, thus facilitating a smooth transition from the backward stroke to the forward stroke.

To quantitatively assess the capabilities of air hammers with combined air distribution systems (see Fig. 4), a numerical analysis of their operating cycles was performed. Similar to the study of typical air distribution diagrams presented above, the design dimensions of all three air hammers were standardized to the same size as a DTH hammer with an outer body diameter of 70 mm.

### Results of simulation modeling of the operating cycle of DTH hammer designs with combined air distribution systems

The numerical study and the search for optimal settings of DTH hammer parameters were conducted using the methodology described earlier. For a more detailed examination of the mechanical diagram of the ring elastic valve integrated into the comprehensive computational model of the air percussion machine, additional information can be found in [18]. Table 5 provides the initial calculation conditions, design parameter values, and output design parameters of the air hammers. The diagrams illustrating the operating cycle can be referred to in Fig. 5.

The results of simulating air hammers with elastic valves (P105-2K, K1, K2 diagrams) have demonstrated the stable operation of these devices, with the valves effectively fulfilling their functions. In all air distribution systems employing elastic valves,

Table 5

Design parameters of combined air percussion systems for lightweight DTH hammers

Prototype machine	M29T					
Air percussion system diagram	P105-2K		K1		K2	
Air distribution type	Valve-spoolless		Valve-spoolless		Valve-throttle	
Specified parameters						
Overpressure in the main line $p_m$ , MPa	0.5	0.6	0.5	0.6	0.5	0.6
Bit diameter, mm	85		85		85	
Outer diameter of the body (cylinder), mm	70		70		70	
Inner diameter of the body (max / min), mm	56 / 56		56 / 47		56 / 47	
Total length of air hammer with bit $L$ , mm	534		534		534	
Hammer mass $m_1$ , kg	1.75		1.75		1.75	
Effective area of hammer (BSC/FSC) $S_{ij}$ , cm <sup>2</sup>	23.3 / 23,3		24.1 / 23.3		24.1 / 23.3	
Ratio of effective area (FSC) of hammer to cross-section area of body with a diameter of 70 mm	0.61		0.61		0.61	
Dimensional stroke $H_d$ , mm	77		77		77	
Flow rate coefficient $k_f$	0.5–0.6		0.5–0.6		0.5–0.6	
Velocity recovery coefficient $k_v$	1.10–0.15		0.10–0.15		0.10–0.15	
Stroke before exhaust from BSC, mm	46		32		32	
Chamber initial volumes: $V_1$ , dm <sup>3</sup> ; $V_2$ , dm <sup>3</sup> ; $V_3$ , dm <sup>3</sup> ; $V_4$ , dm <sup>3</sup>	0.0380; 0.1750; 0.1100; 0.0220		0.0146; 0.1620; 0.0230; 0.0080		0.0146; 0.1620; 0.0230; 0.0080	
Main line channel area $J_{m0}$ , cm <sup>2</sup>	8.04		8.04		8.04	
Area of throttle channel in hammer $J_{13}$ , cm <sup>2</sup>	–		–		0.25	
Hammer/cylinder clearance area, cm <sup>2</sup>	0.04		0.04		0.04	
Area of channel in bit $J_{cha}$ , cm <sup>2</sup>	0.502		0.502		0.502	
Output indicators						
Stroke velocity $v$ , m/s	8.26	9.03	7.58	8.16	7.40	8.06
Operating stroke $H_o$ , mm	67	66	69	69	69	69
Percussion energy $A$ , J	59.7	70.9	50.3	58.3	47.9	56.8
Percussion frequency $f$ , Hz	25.64	27.77	23.8	25.6	22.7	24.4
Cycle period $T_c$ , s	0.039	0.036	0.042	0.039	0.044	0.041
Percussion power $N$ , kW	1.530	1.968	1.196	1.494	1.087	1.386
Total air consumption $Q$ , m <sup>3</sup> /min	3.14	3.72	1.35	1.47	2.51	3.08
Air flow rate through bit channel $Q_b$ , m <sup>3</sup> /min	0.52	0.53	0.24	0.28	0.37	0.42
Specific air consumption $q$ , m <sup>3</sup> /J, ( $\times 10^{-6}$ )	34.2	31.5	18.8	16.4	38.5	37.0



the pre-percussion pressure impulse that resists the hammer's movement is notably reduced (see Fig. 5) compared to the M29T system (as shown in Fig. 3, a) with a cross-over valve. This reduction results in decreased kinetic energy losses of the hammer before percussion, leading to improved machine efficiency.

The air hammer following the P105-2K diagram offers the advantage of increased energy (59.7 J at  $p_m = 0.5$  MPa) and a higher percussion frequency (25.64 Hz). However, this air hammer features elevated average pressure in the forward stroke chamber (FSC) at 0.46 MPa (as seen in Fig. 5, a), and the pressure just before exhaust is 0.43 MPa. Consequently, there is a limited degree of compressed air expansion in the FSC, leading to significant losses of its energy during exhaust. As a result, this air hammer exhibits increased consumption (specific consumption of  $34.2 \times 10^{-6} \text{ m}^3/\text{J}$  absolute consumption  $3.14 \text{ m}^3/\text{min}$ , as shown in Table 3).

The diagrams for the K1 scheme (Fig. 5, b) reveal closely aligns with the optimal mode. In this configuration, the hammer is supplied with the specified kinetic energy, resulting in a percussion energy of 50.3 J and a percussion velocity of 7.58 m/s. The percussion frequency is maintained at 23.8 Hz, and the necessary working stroke of the hammer, measuring 69 mm, is achieved. Additionally, this scheme effectively reduces resistance to the hammer's movement due to air compression and ensures a higher degree of air expansion, enhancing overall efficiency.

The decrease in percussion power by 21.8% in comparison with the P105-2K diagram is attributed to a reduction in the average pressure in the FSC during the working stroke, while the air hammer of the K1 diagram exhibits a 45% lower specific consumption ( $18.8 \times 10^{-6} \text{ m}^3/\text{J}$ ) When compared with the output indicators of the M29T air hammer, the air hammer of K1 diagram demonstrates an 8% lower percussion

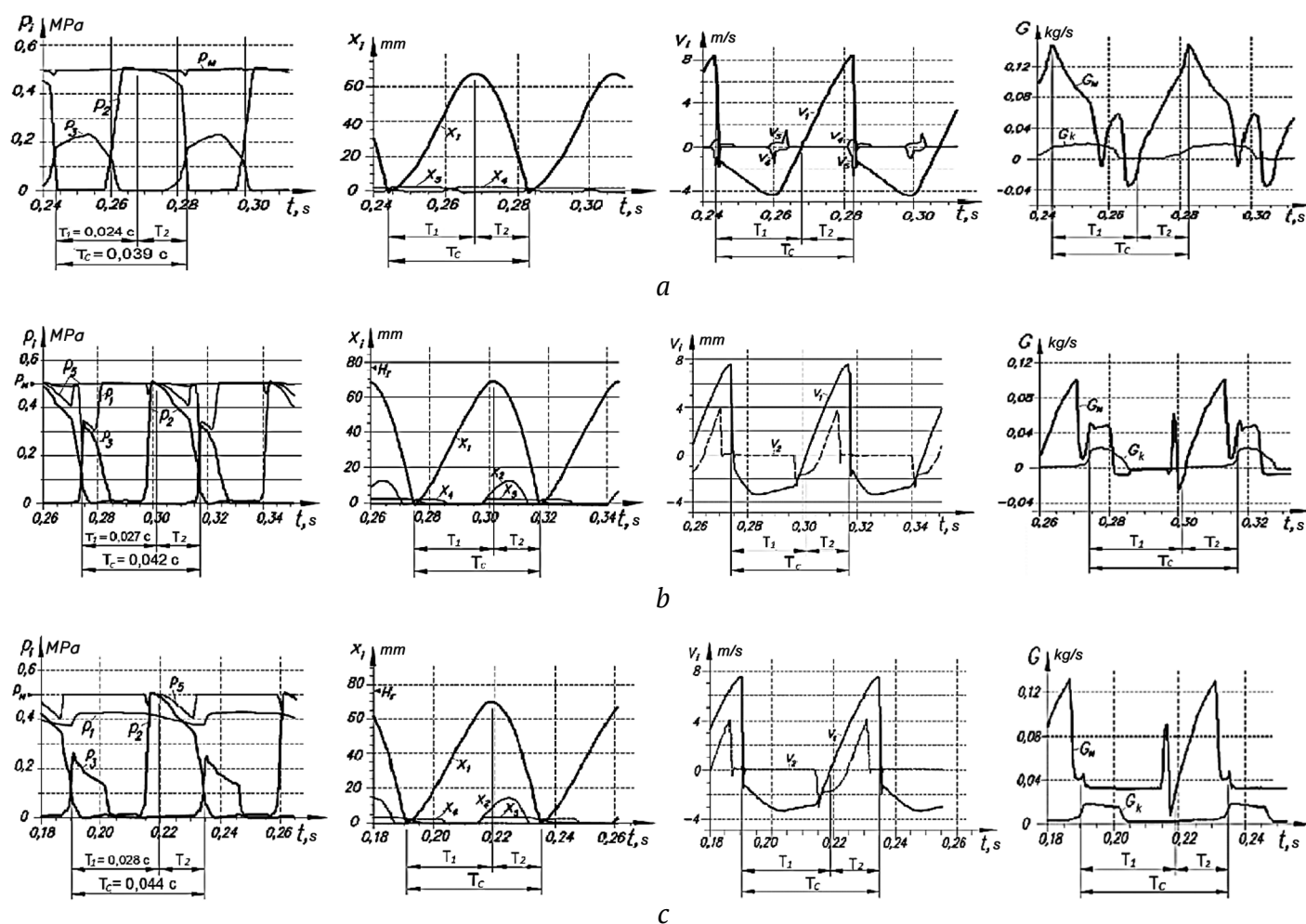


**Fig. 5.** Design diagrams of operating cycles of air hammer models with combined air distribution systems (variations in compressed air pressure in time  $p_i(t)$  in the  $i$ -th chambers; displacement of hammer  $x_1$  and elastic valves  $x_4, x_5$ ; velocity of hammer  $v_1$  and valves  $v_4, v_5$ ; the instantaneous mass flow rate  $G$ :  $G_m$  – instantaneous flow rate through the main channel  $j_{m0}$ ;  $G_{ch}$  – instantaneous flow rate through channel  $j_{cha}$  in the bit): a – air hammer according to the P105-2K diagram; b – according to the K1 diagram; c – according to the K2 diagram:  $t$  – time, s;  $T_c$  – cycle period;  $T_1, T_2$  – periods of backward and forward strokes



power due to a decrease in the frequency of percussions (23.8 Hz), while the specific consumption of K1 is 65% lower.

Simulation results confirm the operational functionality and the lowest specific air consumption for the K1 DTH hammer among the considered devices (refer to Table 5).

The results of simulating the air hammer as per the K2 diagram (Fig. 5, c) demonstrate that the model of the air hammer operates effectively with a cross-sectional area of the throttle channel  $J_{13} \approx 0.25 \text{ cm}^2$ , and with a smaller area ( $J_{13} \leq 0.15 \text{ cm}^2$ ), it does not achieve the required value for the hammer's backward stroke. Key characteristics of the operating cycle are provided in Table 5. In comparison with the K1 diagram, only the diagrams of the instantaneous consumption noticeably differ (as seen in Fig. 5, b, c). The total absolute and specific consumption of the air hammer following the K2 diagram is higher than that of the device adhering to the K1 diagram (see Table 5). Therefore, with the same percussion power, the controllability of channel  $J_{13}$  in the K1 hammer leads to a 2.04-fold reduction in air consumption compared to the K2 hammer. Consequently, it is more advisable to develop air hammers based on the K1 diagram.

In practical applications, it is preferable to utilize the K1 percussion system at a main pressure of

$p_m = 0.6 \text{ MPa}$ , as in this scenario, its percussion power exceeds the design percussion power of the air hammer M29T by 14.9%. However, at  $p_m = 0.5 \text{ MPa}$ , the percussion power of K1 is 8% lower.

Diagrams of the operating cycle of the model K1 at  $p_m = 0.6 \text{ MPa}$  are depicted in Fig. 6. Fig. 6, a presents characteristic sections of the diagrams illustrating hammer displacement  $x_1(t)$  and pressure  $p_i(t)$  during the period of compressed air operation in the forward and backward chambers: 1–2 represents the section of air displacement from the FSC by the hammer during its backward stroke, 2–3 is the period of compressed air intake to the FSC, 3–4 illustrates the air's function in the FSC for expansion before the beginning of exhaust (point 4), 5–6 signifies the period of compressed air intake to the BSC, 6–7 depicts air operation in the BSC for expansion before the beginning of exhaust (point 7).

### Estimation of the compressed air minimum consumption required for bottomhole cleaning

Let us calculate the compressed air consumption,  $\text{m}^3/\text{min}$ , required for cuttings removal, supplied to the bottomhole through the bit channel [21]:

$$Q_b = \frac{0.785 \gamma_r d^2 v_d}{\gamma_a \mu}, \quad (1)$$

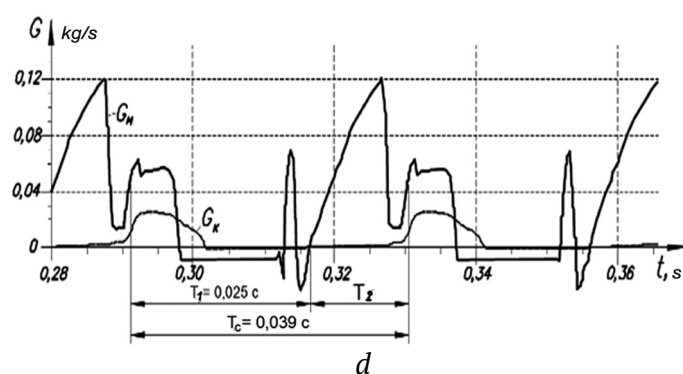
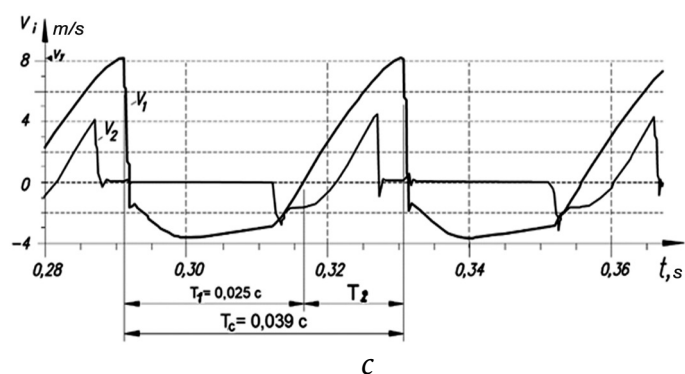
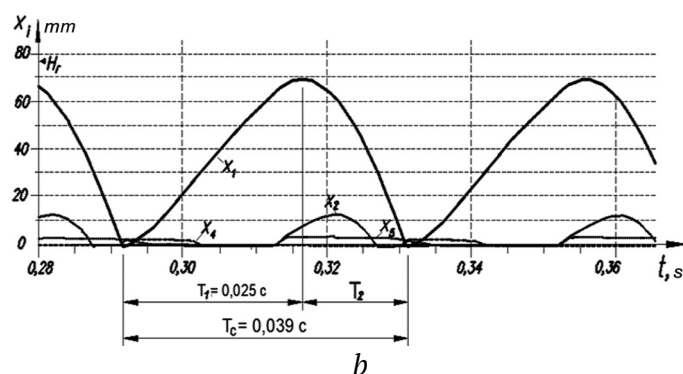
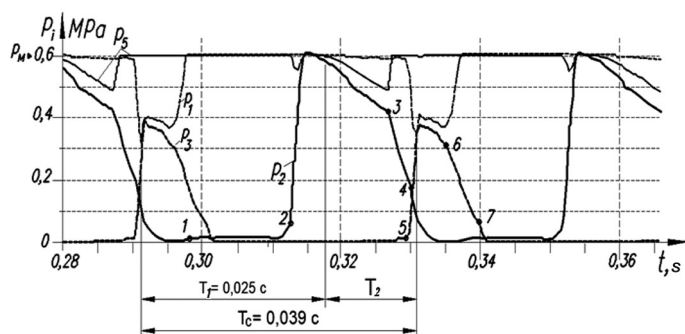


**Fig. 6.** Design diagrams of operating cycles of model K1 air hammer at the main line pressure of 0.6 MPa: a – changes in compressed air pressure in time  $p_i(t)$  in the  $i$ -th chambers (points 1–7 characteristic sections of the diagram); b – displacements of hammer  $x_1(t)$  and valves  $x_2(t)$ ,  $x_4(t)$ ,  $x_5(t)$ ; c – variations in the hammer velocity  $v_1(t)$  and valve velocity  $v_2(t)$ ; d – instantaneous mass flow rate of compressed air  $G(t)$ ;  $t$  – time, s;  $T_c$  – cycle period;  $T_1$ ,  $T_2$  – backward and forward periods;  $G_m$  – flow rate through main line channel  $j_{m0}$ ;  $G_k$  – flow rate through channel  $j_{cha}$  in the bit



where  $\gamma_r$  is the density of the drilled rock, kg/m<sup>3</sup>,  $d$  is the diameter of the borehole (bit), m,  $v_d$  is the mechanical drilling speed, m/min,  $\gamma_a$  is the air density, kg/m<sup>3</sup> (1.2041 kg/m<sup>3</sup> at 20°C),  $\mu$  is the weight concentration of a mixture of fracture products and air ( $\mu = 6$  [19]).

The mechanical drilling speed, m/min, can be determined by formula [10]:

$$v_b = \frac{80An}{d^2f} \cdot \frac{60}{10^6 \cdot 10^3} = 4.8 \cdot 10^{-6} \frac{An}{d^2f}, \quad (2)$$

where  $A$  is the percussion energy, J;  $n$  is the percussion frequency, Hz;  $f$  is the rock hardness coefficient;  $d$  is the borehole (bit) diameter, m;  $4.8 \cdot 10^{-6}$  is the dimensional coefficient.

Substituting (2) into (1), we obtain, m<sup>3</sup>/min:

$$Q_b = 3.768 \cdot 10^{-6} \frac{\gamma_r An}{\gamma_a \mu f}. \quad (3)$$

From (3), we can determine the coefficient of the compressed air consumption, m<sup>3</sup>/min/W, required for bottomhole purging:

$$\psi_b = \frac{Q_b}{An} = 3.768 \cdot 10^{-6} \frac{\gamma_r}{\gamma_a \mu f}. \quad (4)$$

The values of the coefficient  $\psi_b$ , calculated by formula (4), are as follows: for basalt ( $f = 20$ ,  $\gamma_r = 2600$  kg/m<sup>3</sup>)  $\psi_b = 63 \cdot 10^{-6}$  m<sup>3</sup>/min/W, for granite and marble ( $f = 10$ ,  $\gamma_r = 2600$  kg/m<sup>3</sup>)  $\psi_b = 125 \cdot 10^{-6}$  m<sup>3</sup>/min/W, for iron ore ( $f = 6$ ,  $\gamma_r = 3440$  kg/m<sup>3</sup>)  $\psi_b = 276 \cdot 10^{-6}$  m<sup>3</sup>/min/W.

The air hammer (K1) with a percussion power of 1.494 kW, when drilling rock of medium hardness ( $f = 6$ ,  $\gamma_r = 3440$  kg/m<sup>3</sup>), should provide a minimum flow rate through the channel in the bit,  $Q_b = 0.41$  m<sup>3</sup>/min. In harder rocks ( $f = 10$ ,  $\gamma_r = 2600$  kg/m<sup>3</sup>), the minimum flow rate is  $Q_b = 0.1$  m<sup>3</sup>/min, and at  $f = 20$ ,  $\gamma_r = 2600$  kg/m<sup>3</sup>, the minimum flow rate through the bit channel is  $Q_b = 0.09$  m<sup>3</sup>/min.

The calculation results indicate that air hammer K, at  $p_m = 0.6$  MPa and the rock hardness coefficient of  $f = 10$ –20, provides a compressed air flow rate through the bit channel of  $Q_b = 0.28$  m<sup>3</sup>/min, sufficient for cleaning the bottomhole. For rocks with  $f = 6$ , the compressed air intake for borehole purging through the bit channel should be increased by 0.13 m<sup>3</sup>/min. For reliable bottomhole purging, it is advisable to provide a flow rate through the bit of  $Q_b = 0.69$  m<sup>3</sup>/min in air hammer K1, similar to the batch-produced machine M29T. In this case, the total consumption  $Q$  for K1 will be 1.88 m<sup>3</sup>/min, and the total specific consumption is  $q = 21.0 \cdot 10^{-6}$  m<sup>3</sup>/J, which is 51% and 57% lower, respectively, than that of air distribution system M29T.

### Assessment of energy efficiency of a new air hammer

To comparatively assess the energy efficiency of batch-produced M29T and the new K1 air hammers, let us determine the necessary electric power consumed by the compressor when using them:

$$N = nQ, \quad (5)$$

where  $n$  is the specific power of the compressor, kW/(m<sup>3</sup>/min),  $Q$  is the compressed air consumption of the air hammer, m<sup>3</sup>/min.

Given the average value of  $n \approx 5.48$  kW/(m<sup>3</sup>/min)<sup>14</sup>, we obtain the following values of the required electrical power:

- for air hammer M29T:  $N_c = 20.9$  kW;
- for air hammer K1:  $N_c = 10.3$  kW.

Thus, the new air hammer K1 consumes 2.03 times less power than the batch-produced M29T during operation.

### Experimental study of the air percussion mechanism.

#### Assessment of the design models' adequacy

The purpose of the experiments was to obtain experimental data for assessing the adequacy of design models by comparing the indicators of the operating cycle of the air percussion mechanism obtained through physical and numerical simulation. The objectives of the experiments were to record pressure diagrams in the chambers of the device and measure the compressed air consumption. Experimental studies were conducted on a laboratory bench, the diagram and appearance of which are shown in Fig. 7, a, b. The available prototype of the air percussion mechanism of model PM-K2, designed according to the K2 diagram, was used as the research object (see Fig. 4, c).

The percussion device was installed between the work absorber and the power delivery mechanism to balance the recoil of the air percussion mechanism body during its operation. Piezosensors were used to register pressure in the chambers and in the main line. Before each series of experiments, their calibration was performed. The pressure was controlled by a manometer, and the instantaneous flow rate  $G$  of compressed air during the cycles was registered by a flow sensor. The average flow rate of the device was determined by its readings.

In the process of analyzing the experiment results, the percussion energy  $A$ , J, was determined according to the method [20]. The specific compressed

<sup>14</sup> Atlas Copco screw compressors of GA/GA+ series (160–315 kW). URL: [https://aerocompressors.ru/katalog\\_produkcii/kompressori/vintovye\\_elektricheskie\\_kompressory/kompressory\\_atlas\\_copco/kompressor\\_atlas\\_copco\\_ga\\_160-315\\_kv/](https://aerocompressors.ru/katalog_produkcii/kompressori/vintovye_elektricheskie_kompressory/kompressory_atlas_copco/kompressor_atlas_copco_ga_160-315_kv/)

air consumption  $q$ ,  $\text{m}^3/\text{J}$ , was calculated using the formula

$$q = \frac{Q}{60fA}, \quad (6)$$

where  $Q$  is the compressed air consumption,  $\text{m}^3/\text{min}$ ;  $f$  is the frequency of percussions,  $\text{Hz}$ , and  $A$  is the percussion energy,  $\text{J}$ .

The experiments demonstrated the stable operation of the laboratory prototype PM-K2, and experimental pressure diagrams are presented in Fig. 7, *c*, *Experimental*. The following parameters of the operating cycle were established: percussion energy – 630 J, percussion frequency – 8.6 Hz, air consumption –  $7.57 \text{ m}^3/\text{min}$ , percussion power  $N = 5418 \text{ W}$ , and specific consumption  $23.3 \cdot 10^{-6} \text{ m}^3/\text{J}$ .

Under identical experimental conditions, the operating cycle of the PM-K2 was also investigated using the simulation model. A comparison of the experimental data (see Fig. 7, *c*, *Experimental*) and the simulation results (Fig. 7, *c*, *Calculated*) shows that they are nearly identical, sharing the same qualitative and quantitative characteristics. The pressure diagrams ( $p_2$ ,  $p_3$ , as seen in Fig. 7) illustrate a significant degree of air

expansion in the working chambers: the pressures before exhaust in the experiment are  $p_2 = 0.35\text{--}0.41 \text{ MPa}$ , and  $p_3 = 0.2 \text{ MPa}$ , while in the simulation, they are  $p_2 = 0.25\text{--}0.30 \text{ MPa}$  and  $p_3 = 0.15 \text{ MPa}$ . The pressure curves for  $p_0$  and  $p_5$  indicate that the cut-off valve is activated before exhaust, preventing air leakage from the main line into the atmosphere.

To further confirm the adequacy of the design models, experimental data for the M29T air hammer were also used, which were obtained from publications [10, 11]. The technical parameters of air percussion mechanisms M29T and PM-K2 are summarized in Table 6.

The data presented in Table 6 demonstrate that the deviations between the calculated values and the experimental ones are within an acceptable range, with deviations of up to 6% for percussion frequency, 1% for percussion energy, 5% for total compressed air consumption, and 8% for specific compressed air consumption. These comparison results affirm the alignment of the calculated and experimental operating cycles of the air percussion devices being studied. Consequently, the adequacy of the calculation models employed in this research has been validated.

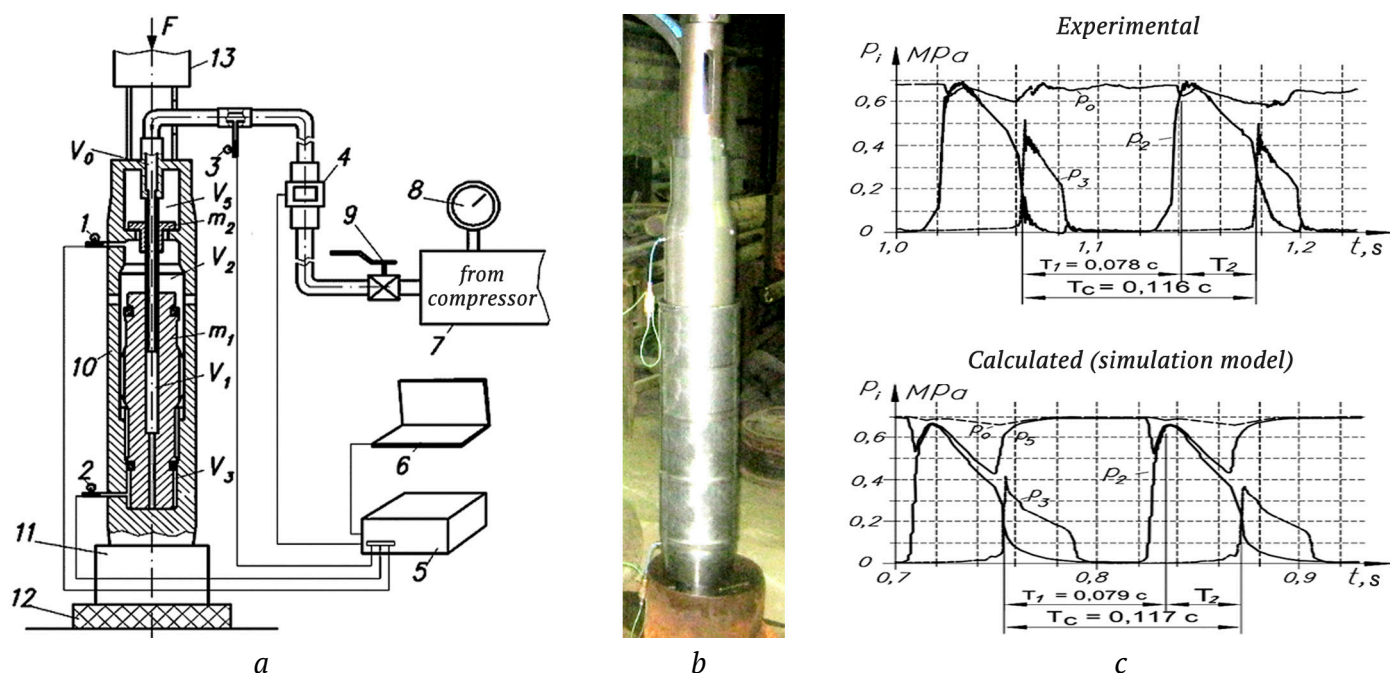


**Fig. 7.** Measurement of pressure in working chambers of air percussion mechanism PM-K2 with two elastic valves on the hammer and compressed air supply cut-off valve to the controllable FSC: *a* – pressure sensors, flow meters, and measuring equipment installation diagram; *b* – laboratory prototype’s appearance with pressure sensors installed, *c* – diagrams of pressure (Experimental, Calculated) in chambers of the laboratory prototype at a pressure in the main line of 0.7 MPa: 1, 2 – pressure sensors (piezosensor of the Kistler instrumente AG company type 701A) in the working and backward stroke chamber; 3 – pressure sensor in the main line; 4 – flow meter (Digital flow switch PF2A706H), 5 – ADC (analog-to-digital converter), 6 – PC (personal computer), 7 – receiver, 8 – pressure gauge, 9 – main line valve, 10 – percussion unit, 11 – adapter, 12 – work absorber, 13 – power delivery mechanism;  $F$  – delivery force,  $V_i$  – working chambers,  $m_i$  – moving components (hammer, cut-off valve);  $p_2$  – pressure in the controllable FSC,  $p_3$  – pressure in the BSC,  $p_0$  – pressure in the main FSC,  $p_5$  – pressure in chamber  $V_5$





Table 6

Comparison of experimental and design technical indicators of air percussion machines

Indicator	M29T				PM-K2		
	Designed	Experimental		Deviation, % (from [11])	Designed	Experimental	Deviation, %
		[11]	[10]				
Main line pressure (g) design $p_m$ , MPa	0.5	0.5	0.5	–	0.7	0.7	–
Hammer mass $m_1$ , kg	1.75	1.75	1.60	–	34.5	34.5	–
Bit channel $J_{cha}$ , cm <sup>2</sup>	0.502				0	–	–
Channel area $J_{13}$ , cm <sup>2</sup>	–	–	–	–	–	0.453	–
Cycle period $T_c$ , s	0.038	0.040	0.035	–5.0	0.117	0.116	+0.9
Period of backward stroke $T_1$ , s	0.023	–	–	–	0.079	–	–
Period of forward stroke $T_2$ , s	0.015	–	–	–	0.039	–	–
Operating stroke of hammer $H_0$ , mm	67	–	–	–	134	–	–
Stroke velocity $v$ , m/s	7.86	7.86	7.83	0.0	6.02	6.05	–0.5
Percussion energy $A$ , J	54.0	54.0	49.0	0.0	625	630	–0.8
Percussion frequency $n$ , Hz	26.3	25.0	28.3	+5.2	8.55	8.6	–0.6
Percussion power $N$ , kW	1.42	1.35	1.39	+5.2	5.34	5.42	–1.4
Flow rate through bit $Q_b$ , m <sup>3</sup> /min	0.69	–	–	–	0	0	–
Total consumption $Q$ , m <sup>3</sup> /min	3.81	4.00	4.50	–4.8	7.85	7.57	+3.7
Specific consumption $q$ , m <sup>3</sup> /J ( $\times 10^{-6}$ )	44.7	44.4	53.9	+0.7	24.5	23.3	–7.5

## Conclusion

1. Energy conservation in the mining industry and the maintenance of required compressed air pressure in underground mining networks can be achieved by reducing the specific air consumption of down-the-hole hammers.

2. Analysis of operating cycles of typical air distribution systems for air hammers, including valve-operated, spoolless, and spool-operated systems, has revealed conditions for ensuring the economic efficiency of an air percussion system. These conditions include eliminating pneumatic resistance to the hammer's movement and increasing the degree of air expansion in the working chambers.

3. A proposed air distribution system that meets the above requirements includes two elastic valves on the hammer, a cut-off valve for controlling compressed air supply to the forward stroke chamber, and controlled inlet to the backward stroke chamber.

4. An air hammer has been developed based on this air distribution system, designed to be the same size as the batch-produced machine M29T. Numerical simulations have determined its optimal design parameters, emphasizing specific consumption. Calculations show that, despite its similar dimensions and percussion power to M29T, the designed hammer consumes 53% less specific energy and requires 2 times less electric power for compressed air supply.

5. A comparison of the design data, experimental data, and literature sources has demonstrated qualitative and quantitative similarity between experimental and design diagrams of the operating cycle. The deviations of calculated parameters from experimental data are within acceptable limits, with variances of up to 6% for percussion frequency, 1% for percussion energy, 5% for absolute compressed air consumption, and 8% for specific compressed air consumption. This confirms the adequacy of the calculation models and the accuracy of the calculation results.

## References

1. Mineeva A.S. Energy efficiency as a factor of sustainable development for a mining company. *Journal of Economy and Entrepreneurship*. 2016;(11–2):565–570. (In Russ.)
2. Lyukhanov V.V., Alferov S.B., Trofimov S.N., Rozhentsov V.F. Pneumatic high-pressure rock drill by Nipigormash OAO and Mashinostroitelny Holding ZAO. *Russian Mining Industry*. 2012;(5): 28–30. (In Russ.)
3. Smolyanitsky B.N., Repin A.A., Danilov B.B. et al. *Improving the efficiency and durability of impulse machines for the construction of long wells in rock masses*. Monograph. Novosibirsk: SB RAS Publ.; 2013. 204 p. (In Russ.)
4. Karpov V.N., Nemova N.A., Reznik A.V. On improving the efficiency of drilling blast wells in the development of solid minerals. In: *Innovations and prospects for the development of mining engineering*





and electromechanics: a Collection of Abstracts of the 8<sup>th</sup> International Scientific and Practical Conference. St. Petersburg: SPGU; 2021. Pp. 341–345. (In Russ.)

5. Kumykova T.M., Kumykov V.K. Dynamics of mine hydro-pneumatic accumulator. *Journal of Mining Science*. 2013;49(5):763–771. <https://doi.org/10.1134/S1062739149050109> (Orig. ver.: Kumykova T.M., Kumykov V.K. Dynamics of mine hydro-pneumatic accumulator. *Fiziko-Tekhnicheskiye Problemy Razrabotki Poleznykh Iskopayemykh*. 2013;(5):99–109. (In Russ.))

6. Alekseev S.E., Kokoulin D.I. The use of down-the-hole hammers for straight directional drilling. In: *Modern problems in mining and methods of modeling mining and geological conditions in the development of mineral deposits: proceedings of the All-Russian scientific and tech. conf. with international participation*. Kemerovo RF, 2015. Kemerovo: TF Gorbachev Kuzbass State Technical University; 2015 (In Russ.)

7. Gaun V.A. Development and research of down-the-hole hammers with increased impact energy. In: *Improving the efficiency of pneumatic percussion drilling machines: a collection of scientific papers*. Novosibirsk: Institute of Mining SB USSR AS; 1987. Pp. 3–10. (In Russ.)

8. Lipin A.A. Promising pneumatic punchers for borehole drilling. *Journal of Mining Science*. 2005;41(2):157–161. <https://doi.org/10.1007/s10913-005-0078-0> (Orig. ver.: Lipin A.A. Promising pneumatic punchers for borehole drilling. *Fiziko-Tekhnicheskiye Problemy Razrabotki Poleznykh Iskopayemykh*. 2005;(2):74–78. (In Russ.))

9. Emelyanov P.M., Esin N.N., Zinoviev A.A. et al. *Machines for drilling boreholes with down-the-hole hammers in underground conditions*. Novosibirsk: SB USSR AS; 1965. (In Russ.)

10. Ivanov K.I., Latyshev V.A., Andreev V.D. *Drilling technique in the mineral deposit mining*. Moscow: Nedra Publ.; 1987. 272 p. (In Russ.)

11. Sudnishnikov B.V., Esin N.N., Tupitsyn K.K. *Study and designing of pneumatic impact machines*. Novosibirsk: Nauka Publ.; 1985. 134 p. (In Russ.)

12. Wijk G. (Ed.) *Hammer theory and practice*. 2008. URL: [https://www.researchgate.net/publication/271527406\\_Hammer\\_Theory\\_and\\_Practice](https://www.researchgate.net/publication/271527406_Hammer_Theory_and_Practice)

13. Gerts E.V. *Pneumatic drives. Theory and calculation*. Moscow: Mashinostroenie Publ.; 1969. 359 p. (In Russ.)

14. Myuntser E.G. Construction of a mathematical model of pneumatic impact mechanisms on a computer. In: *Pneumatic drilling machines: collection of scientific papers*. Novosibirsk: Institute of Mining SB USSR AS; 1984. p.49–55. (In Russ.)

15. Fedulov A.I., Arkhipenko A.P., Mattis A.R. *Selection of gaps in the rubbing pairs of a pneumatic hammer*. Novosibirsk: Siberian dept. of Nauka publ; 1980. 128 p. (In Russ.)

16. Petreev A.M., Primychkin A.Y. Ring-type elastic valve operation in air hammer drive. *Journal of Mining Science*. 2016;52(1):135–145. <https://doi.org/10.1134/S1062739116010224> (Orig. ver.: Petreev A.M., Primychkin A.Y. Ring-type elastic valve operation in air hammer drive. *Fiziko-Tekhnicheskiye Problemy Razrabotki Poleznykh Iskopayemykh*. 2016;(1):132–143. (In Russ.))

17. Tambovtsev P.N. Experimental studies of pneumatic impact device with a reduced specific consumption of compressed air. *Fundamental and Applied Issues of Mining*. 2020;7(2):47–52. (In Russ.) <https://doi.org/10.15372/FPVGN2020070208>

18. Petreev A.M., Primychkin A.Y., Vorontsov D.S. Ring-shape elastic valve in the air percussion machines. *Journal of Mining Science*. 2010;46(4):416–424. <https://doi.org/10.1007/s10913-010-0052-3> (Orig. ver.: Petreev A.M., Primychkin A.Y., Vorontsov D.S. Ring-shape elastic valve in the air percussion machines. *Fiziko-Tekhnicheskiye Problemy Razrabotki Poleznykh Iskopayemykh*. 2010;(4):56–65. (In Russ.))

19. Tymchur A.D. On the issue of improving the pneumatic transport of drill chips when drilling holes in open pits. *Proceedings of USGU*. 2000;(11):277–279. (In Russ.)

20. Esin N.N. *Methods of research and fine-tuning of pneumatic hammers*. Novosibirsk: Institute of Mining SB USSR AS; 1965. 76 p. (In Russ.)

### Information about the authors

**Pavel N. Tambovtsev** – Cand. Sci. (Eng.), Associate Professor, Senior Researcher of the Impulse Systems Modeling Laboratory, N.A. Chinakal Institute of Mining of the Siberian Branch of the RAS, Novosibirsk, Russian Federation; ORCID [0000-0003-1058-2764](https://orcid.org/0000-0003-1058-2764), Scopus ID [7004038110](https://orcid.org/7004038110); e-mail [tambovskiyp@mail.ru](mailto:tambovskiyp@mail.ru)

**Evgeny P. Rusin** – Cand. Sci. (Eng.), Senior Researcher of the Department of Mining and Construction Geotechnics, N.A. Chinakal Institute of Mining of the Siberian Branch of the RAS, Novosibirsk, Russian Federation; ORCID [0000-0001-7220-8589](https://orcid.org/0000-0001-7220-8589), Scopus ID [20434728100](https://orcid.org/20434728100); e-mail [gmmlab@misd.ru](mailto:gmmlab@misd.ru)

Received 14.12.2022

Revised 31.07.2023

Accepted 25.09.2023